on the mechanisms of UV-B resistance in plants (*26*). UV-B intensity also varies widely with season, latitude, and altitude. Like resistance to other environmental stresses such as drought or cold, the degree of tolerance of a particular plant species to UV-B may influence the range of environments at which certain plant species can survive. We have shown that the ability to efficiently repair (6-4) photoproducts is an essential component of UV-B resistance in *Arabidopsis*.

REFERENCES AND NOTES

1. V. Walbot, *Trends Genet.* 1, 165 (1985).
2. E. J. Klekowski, *Mutation, Developmental Selection, and Plant Evolution* (Columbia Univ. Press, New York, 1988).
3. G. D. Small, *Mutat. Res.* **181**, 31 (1987).
4. J. Veleminsky and K. Angelis, in *Mutation and the Environment*, R. Mortimer, L. Mendelsohn, R. Albertini, Eds. (Wiley-Liss, New York, 1990), vol. 340, pp. 195–203.
5. D. Karentz, J. E. Cleaver, D. L. Mitchell, *J. Phycol.* **27**, 326 (1991).
6. A. G. McLennan, *Mutat. Res.* **181**, 1 (1987).
7. Q. Pang and J. B. Hays, *Plant Physiol.* **95**, 536 (1991).
8. M. Koornneff, Arabidopsis *Inf. Serv.* **27**, 1 (1990).
9. A. R. Kranz and B. Kirchheim, in *Genetic Resources in* Arabidopsis, A. R. Kranz, Ed. (*Arabidopsis* Information Service, Botanical Institute, J. W. Goethe-University, Frankfurt, 1987), vol. 24, p. 421.
10. M. Koornneef *et al.*, *J. Hered.* **74**, 265 (1983).
11. *ISCO Tables* (Instrumentation Specialties Company, Lincoln, NE, 1970).
12. D. L. Mitchell, C. A. Haipek, J. M. Clarkson, *Mutat. Res.* **143**, 109 (1985).
13. V. A. Bohr, C. A. Smith, D. S. Okumoto, P. C. Hanawalt, *Cell* **40**, 359 (1985).
14. D. C. Thomas, D. S. Okumoto, A. Sancar, V. A. Bohr, *J. Biol. Chem.* **264**, 18005 (1989).
15. D. L. Mitchell and R. S. Nairn, *Photochem. Photobiol.* **49**, 805 (1989).
16. W. A. Franklin and W. A. Haseltine, *Mutat. Res.* **165**, 1 (1986).
17. D. E. Brash and W. A. Haseltine, *Nature* **298**, 189 (1982).
18. J. E. Cleaver *et al.*, *Mol. Cell. Biol.* **7**, 3353 (1987).
19. M. Z. Zdzienicka *et al.*, *Mutat. Res.* **273**, 73 (1992).
20. L. H. Thompson *et al.*, *Mutagenesis* **4**, 140 (1989).
21. W. A. Franklin and W. A. Haseltine, *Proc. Natl. Acad. Sci. U.S.A.* **81**, 3821 (1984).
22. A. Sancar and W. D. Rupp, *Cell* **33**, 249 (1983).
23. D. E. Brash, W. A. Franklin, G. B. Sancar, A. Sancar, W. A. Haseltine, *J. Biol. Chem.* **260**, 11438 (1985).
24. J. E. Frederick and D. Lubin, *Photochem. Photobiol.* **47**, 571 (1988).
25. F. E. Quaite, B. M. Sutherland, J. C. Sutherland, *Nature* **358**, 576 (1992).
26. A. Stapleton, *Plant Cell* **4**, 1353 (1992).
27. R. A. Fisher and B. Balmukand, *J. Genet.* **20**, 79 (1928).
28. R. W. Allard, *Hilgardia* **24**, 235 (1956).
29. M. Shure, S. Wessler, N. Fedoroff, *Cell* **35**, 225 (1983).
30. A. K. Ganesan, C. A. Smith, A. A. van Zeeland, in *DNA Repair*, E. C. Freidberg and P. C. Hanawalt, Eds. (Dekker, New York, 1981), vol. 1A, pp. 89–98.

31. The authors thank T. Murphy, A. Smith, and M. Learned for their valuable advice and encouragement. We also thank A. Ganesan for the T4 endonuclease V and A. Lloyd and M. Koornneef for supplying mutants of *Arabidopsis*. Supported by grant DMB-90-19159 from the NSF, Division of Molecular Biosciences.

22 March 1993; accepted 30 July 1993

Major Groove Accessibility of RNA

Kevin M. Weeks* and Donald M. Crothers

Chemical acylation experiments showed that the RNA major groove, often assumed to be too deep and narrow to permit recognition interactions, is accessible at duplex termini. Reactivity extended further into the helix in the 5′ than in the 3′ direction. Asymmetric and large loops between helices uncoupled them, which yielded both enhanced reactivity at terminal base pairs and weaker stabilization enthalpy compared to that in small loops or symmetric loops of the same size. Uncoupled helices have effective helix ends with accessible major grooves; such motifs are attractive contributors to protein recognition, tertiary folding, and catalysis.

The geometry of the RNA helix determines, in part, the recognizability of the major and minor grooves (*1*). In a continuous A-form RNA helix, the minor groove is wide and shallow, which facilitates the interaction of base functional groups with complementary ligands. In contrast, the major groove is deep and narrow and may be inaccessible for specific recognition. This fundamental consequence of RNA geometry presents a paradox: the inaccessible major groove presents a richer ensemble of arrayed hydrogen bond acceptors and donors than the minor groove does (*2*). Given the ubiquity of helical segments in RNA and the limits imposed by having only four constituent subunits, many distinguishing interaction surfaces are potentially buried in the major groove.

Despite this prediction, there are several well-characterized examples of RNA recognition achieved by way of interaction in the major groove. The tertiary folding of transfer RNA (tRNA) uses base triplets in which a third nucleotide forms hydrogen bonds with a Watson-Crick base pair in the major groove of short helices (*3*); the guanosine binding site in the *Tetrahymena* ribozyme is located in the major groove at the end of a short, bulged helix (*4*); the yeast aspartyl-tRNA synthetase contacts both the acceptor and anticodon stems from the major groove side (*5*); and peptide models for the RNA binding domain of the human immunodeficiency virus (HIV) Tat protein bind TAR RNA at the major groove adjacent to a bulge loop (*6*, *7*). Major groove inaccessibility is a consequence of the close approach of the phosphoribose backbones for helices of six or more base pairs (bp) (*8*). Accessibility in the major groove might be modulated where this regularity is interrupted.

Diethyl pyrocarbonate (DEPC) carbethoxylates purines primarily at the N7 position in a reaction sensitive to the solvent exposure of the base (*6*, *9*). DEPC has an effective diameter of ~3.5 Å (*10*), which is similar to the width of the deep RNA major groove (~4 Å). DEPC is comparable in size to amino acid and nucleotide motifs that mediate RNA-protein or RNA-RNA interactions; hence, the reactivity rates of this probe reflect the steric accessibility and thus the recognizability of individual purine nucleotides.

Our experiments establish a correlation between DEPC reactivity, which reflects accessibility of the major groove, and the presence of either true or effective helix ends. Effective ends result when adjacent helices are separated by loops that decouple them thermodynamically, as reflected in a diminished enthalpy of melting. We find, in agreement with Peritz *et al.* (*11*), that asymmetric loops are more effective than symmetric loops in lowering overall thermal stability and show that major groove accessibility is relatively enhanced at helix ends that flank asymmetric (and large) loops. These structures constitute an RNA motif capable of specific interaction in the major groove.

RNA duplexes that incorporate simple bulge and internal loops were generated by pairwise combination of 10 synthetic oligoribonucleotides (Fig. 1) (*12*). Duplexes were designed to simplify the experimental protocol and feature a homopurine strand uniquely susceptible to attack by DEPC. All helices include 20 bp and predominantly adenosine bases, which are more reactive toward DEPC (*9*), and include terminal and internal G-C base pairs to prevent fraying and ensure proper duplex register, respectively. Helices are identified by the number of unpaired or mismatched cytosine nucleotides in the center of the duplex. For example, the perfect 20-bp duplex is identified as [00], whereas a dinucleotide bulge on the right hand (pyrimidine) strand is [02] (Fig. 1).

In the absence of complementary oligonucleotides, the 10 single strands (Fig.

Department of Chemistry, Yale University, New Haven, CT 06511.

*Present address: University of Colorado, Department of Chemistry and Biochemistry, Boulder, CO 80309.

1) show broad, relatively featureless melting transitions. All 25 duplexes yield sharp transitions consistent with helix melting (*13*), from which the destabilizing free energy due to the defect, $\Delta\Delta G°$, and the van't Hoff transition enthalpy, $\Delta H°_{vH}$, can be evaluated (*14*). Our thermodynamic data are in quantitative agreement with prior work on the contribution of internal defects to duplex stability (*11, 15*).

Asymmetric defects are more destabilizing than symmetric loops containing the same number of unbonded nucleotides (Fig. 2). For loop size $n = 2$, [11] is more stable than [02] or [20] by 2.3 kcal/mol at 37°C. Analogously, [22] is 1.4 kcal/mol more stable than [13] or [31] and is even more stable than the smaller loops [02] or [20] ($\Delta\Delta G° \approx 2.0$ kcal/mol). Similar comparisons can be deduced from Fig. 2. In addition, duplexes with the same defect on opposite strands are similarly destabilized; for example, [01] and [10] or [35] and [53] have the same thermodynamic properties within experimental error.

There is a significant difference in the enthalpy (which reflects stacking interactions) that stabilizes molecules with symmetric defects compared to the enthalpy that stabilizes asymmetric loops. The van't Hoff transition enthalpies for [00], [11], and [22] are comparable (~−155 kcal/mol) and are more negative (stabilizing) than those of asymmetric and larger loops. These data suggest that asymmetric loops disrupt stacking between the two helices but that stacking is maintained across small symmetric loops. Values for $\Delta H°_{vH}$ approach a plateau value of about -133 ± 6 kcal/mol for loops with asymmetry greater than two nucleotides or loop size greater than approximately seven nucleotides (Fig. 2). This is an expected result because the interaction enthalpy should be constant once stacking across the defect is completely disrupted.

We term helices that have lost the enthalpy of stacking across an intervening defect uncoupled. Relative free energies for uncoupled helices (Fig. 2) are well accounted for by Jacobson-Stockmayer (JS) theory, which assumes that a random flights chain model (incorporating an excluded volume effect) accounts for the entropy of loop closure in molecules that contain defects (*16*). Small symmetric loops are strongly coupled, as reflected in their greater stability and more negative enthalpy of formation, but become less so as their size increases. The limiting behavior of uncoupled loops is approached even by symmetric loops when n is approximately 10.

Treatment (*17*) of the homopurine strands [L1] to [L3] or [L5] with DEPC yields an even pattern of intensity at each chain position primarily modulated by the stronger intrinsic reactivity of the N7 position of adenosine compared to that in guanosine bases ([L0+], [L1+], [L2+], and [L3+]) (Fig. 3). In contrast, DEPC susceptibility in each of the RNA duplexes is strongly modulated by position relative to helix termini and bulge or internal loops (compare [00], [01], [02], and [03] in Fig. 3). The uninterrupted helix [00] is essentially unreactive at internal base pairs. Reactivity toward DEPC increases smoothly near helix termini and adjacent to specific classes of internal defects.

The relative reaction rate, termed accessibility (α_i), is defined as the ratio of the rate of cleavage of the double-stranded RNA to the rate at the same position i in the single-stranded oligoribonucleotide ($\alpha_i = k_i^{ds}/k_i^{ss}$) and was determined from gels like that shown in Fig. 3 (*18*). Thus, if a given nucleotide is as accessible in the duplex as in the single strand, α_i equals 1. In general, α_i is less than 1; accessibility in regions completely occluded by an uninterrupted phosphoribose backbone is ~0.03. We plotted accessibilities on a logarithmic scale to reflect the difference in the free energy of activation ($\Delta G^{\ddagger}$) for DEPC attack at a base-paired versus single-stranded nucleotide ($\log \alpha_i \propto \Delta G_i^{\ddagger ds} - \Delta G_i^{\ddagger ss}$ + constant) (Fig. 4).

Inspection of the accessibility of the RNA duplexes reveals a consistent pattern of accessibility at helix termini (Fig. 4). The 5′ terminal purine in the duplex is approximately one-half as accessible as the corresponding position in the single-stranded oligonucleotide. Increased acces-

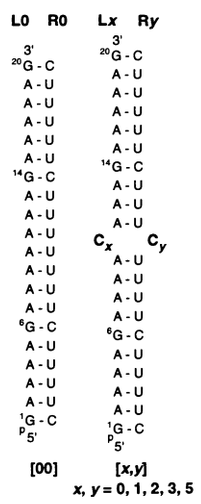

Fig. 1. Secondary structures of model RNA duplexes. Duplexes are formed by pairwise combination of the single-stranded oligoribonucleotides [L0] through [L3], [L5], [R0] through [R3], and [R5]. The position of the 5′ radiolabel is indicated by a small "p." Nonradiolabeled oligos have 5′ and 3′ hydroxyl termini. The wild-type oligonucleotide is on the left; L, left; R, right.

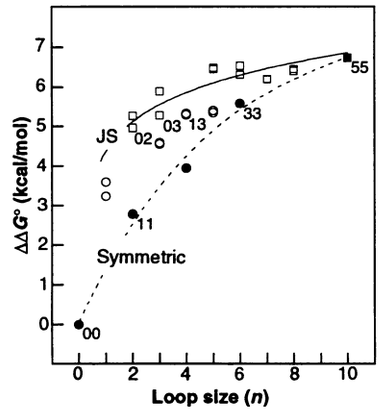

Fig. 2. Internal loop free energy as a function of loop size. Values for $\Delta\Delta G°$ are equal to $\Delta G°_{37°C}$ [00] − $\Delta G°_{37°C}$ (defect-containing helix). Symmetric and asymmetric internal loops are shown as solid and open symbols, respectively; enthalpically uncoupled helices (those with $\Delta H°_{vH} = -133 \pm 6$ kcal/mol) are indicated with squares. Representative duplexes are identified explicitly. The line marked JS corresponds to the limiting behavior expected for a chain in which the cost of loop closure is entropic [as described by Jacobson-Stockmayer theory (*16*)] with $c = 1.75$ and $\Delta S_{geo} = 14.1$ cal/mol.

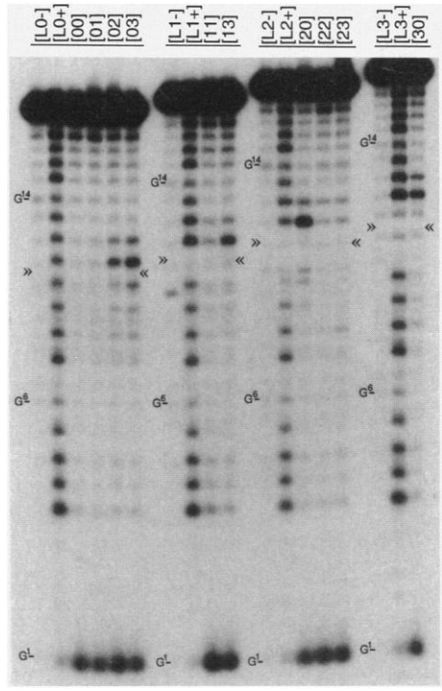

Fig. 3. Accessibility of DEPC to base-paired versus single-stranded RNA. Here, the reaction of the representative single-stranded homopurine oligonucleotides [Lx+] with DEPC for 10 min at 20°C is compared with 60-min modification of the same 5′ ^{32}P-labeled strands in the duplexes (identified as shown in Fig. 1). Duplex midpoints (and thus defect positions, where present) are indicated with arrowheads. Oligonucleotides [Lx−] indicate background cleavage from aniline treatment in the absence of DEPC.

sibility at the purine N7 position extends 4 ± 1 and 2 ± 1 nucleotides in from the 3′ and 5′ ends, respectively (Fig. 4A).

Nonterminal purines in the uninterrupted [00] helix are resistant to modification by DEPC, which confirms our expectations that the phosphoribose backbone occludes the floor of the major groove in a continuous A-form helix (*1*). Consistent with previous observations in a different sequence context (6), a single nucleotide bulge enhances accessibility in the major groove only modestly. Positions that abut bulges of more than one nucleotide are readily modified by DEPC (Fig. 4, B and C). The pattern is strongly asymmetric, and like the reaction at helix termini, accessibility extends one to two nucleotides further in the 5′ direction than in the 3′ direction. However, the most accessible position consistently falls at the purine 3′ to the bulge.

Helices flanking the symmetric and thermodynamically coupled (Fig. 2), and thus partially stacked, internal loops [00], [11], and [22] are substantially less susceptible to acylation in comparison to the bulge loops (compare Fig. 4D with 4B and 4C). The single C-C mismatch appears to be readily accommodated within the regular helix as shown by its lack of reactivity toward DEPC. Loops [22] and [33] are moderately accessible at the base 3′ to the internal loop.

Large asymmetric internal loops exhibit two distinct classes of reactivity (Fig. 4, E and F). Most of these helices are partially enthalpically coupled according to the criteria shown in Fig. 2, except for loops [35] and [53], which are uncoupled. One class (Fig. 4E) shows a pattern of strong reactivity similar to bulges of more than one nucleotide. The second class exhibits a more complex pattern (Fig. 4F). These patterns probably reflect stacking, loop conformation, and favorable local interaction or a combination of these factors. These data correlate well with cleavage patterns generated by the bulky major groove intercalator $Rh(phen)_2phi^{3+}$ (*19*), which reacts at stem loop junctions and bulge loops of more than one nucleotide in 5S ribosomal RNA (*19*).

Fraying cannot account for the observed accessibility. First, the equilibrium constants for fraying (K_{fray}) of the terminal base pairs (GA)·(CU) and (AG)·(UC) at 20°C are 0.04 and 0.1, respectively (*20*). The observed accessibilities at helix termini are 13-fold and at least 2-fold greater than this, respectively, and calculated values for K_{fray} incorrectly predict the 3′ purine to be most reactive (Fig. 4), which implies that another mechanism is required to account for the observed reactivity. Second, accessibility is not correlated with melting temperature (T_m): [03], [30], and [33] have similar values for T_m and for the free energy of formation (*13*), although [33] is significantly less susceptible to acylation by DEPC (Fig. 3). Finally, failure to follow a two-state model (of which fraying is one example) may be estimated from the divergence of experimental and theoretical differential melting curves (*14*) below T_m. For most helices, even fraying has not begun at the temperature of the modification experiments. The pre-melting transitions for both [02] and [22] begin at ~25°C, significantly above the modification temperature of 20°C (*13*). Yet, the asymmetric bulge loop [02] is strongly reactive to DEPC, whereas [22] is not.

Structure and major groove recognizability may be evaluated both in terms of the relative contributions of enthalpy and entropy to helix destabilization as compared with an uninterrupted helix and in terms of the reactivity of purine N7 positions. For most helices, our two criteria yield convergent results: (enthalpically) decoupled helices are accessible to acylation in the major groove, and coupled helices are not. We postulate that strongly coupled helices incorporate interhelix defects into a continuation of regular duplex stacking geometry and therefore are inaccessible to DEPC.

Our DEPC susceptibility experiments suggest four guidelines for recognition in the RNA major groove (Fig. 5A); it is expected that these rules must be modified

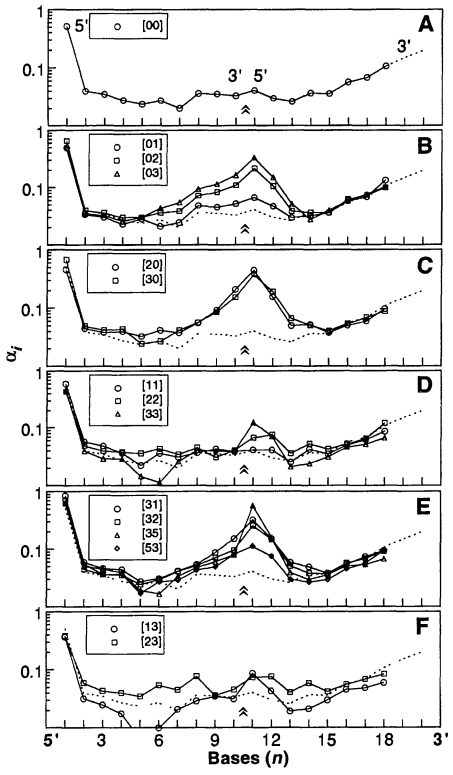

Fig. 4. Quantitative base accessibility. Accessibility (α_j) is plotted on a logarithmic scale as a function of purine position. Accessibility of [00] (**A**) is reproduced in the other panels as a dotted line to permit comparison of the effect of the introduction of a defect of helix accessibility. The two farthest 3′ bases could not be resolved by electrophoresis; accessibility is shown increasing monotonically across these positions. Duplexes are identified individually in each panel. (**B**) Pyrimidine (right) strand bulges. (**C**) Purine (left) strand bulges. (**D**) Symmetric internal loops. (**E** and **F**) Large, asymmetric internal loops.

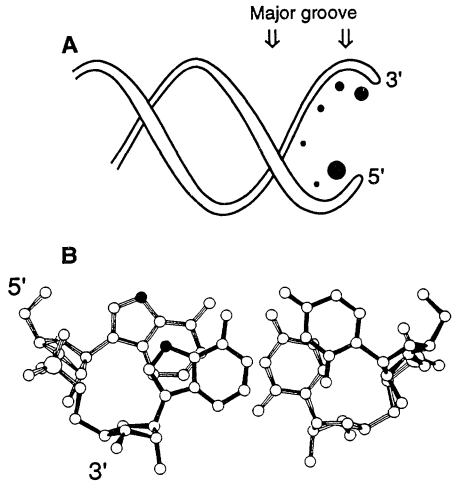

Fig. 5. Summary of base accessibility at helical irregularities compared with A-form geometry. (**A**) Summary of expected accessibility for a theoretical duplex in which accessibility was monitored for all bases on both strands adjacent to a helical irregularity. The diameter of the solid spheres represents the relative accessibility for bases at the positions indicated for a defect located to the right of the idealized helix. (**B**) Consequence of A-form geometry for stacking of RNA base pairs. N7 atoms are filled in.

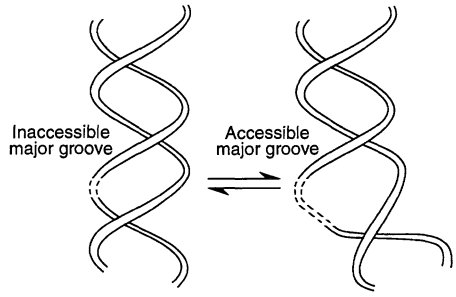

Fig. 6. Major groove accessibility switch. Hypothetical equilibrium between coaxially stacked helixes in which the major groove is expected to be inaccessible and helices in which the phosphoribose backbone regularity is disrupted, thus facilitating interaction in the major groove. The helices shown could be separated by any type of intervening structure. The accessibility switch requires only formation and disruption of coaxial stacking between helices.

to account for the contribution that local folding and tertiary interactions make to overall accessibility. (i) The bases in double-stranded secondary structures not adjacent to helix termini and other irregularities are energetically costly targets for recognition in the major groove (Fig. 4A). Other energetically favorable recognition schemes are possible (*21*). (ii) Helix termini are available for interaction and recognition. This intrinsic accessibility extends further into the major groove in the 5′ direction (from the 3′ end) than in the 3′ direction (approximately 4 ± 1 and 2 ± 1 bases, respectively) (Fig. 5A). (iii) Bulge loops of at least two nucleotides and large or asymmetric internal loops have an effect similar to that of helix termini and greatly increase the recognizability of neighboring bases in the major groove at these effective helix ends. The pattern of susceptibility appears as an approximate superposition of reactivity of two isolated helix termini at these uncoupled junctions. (iv) Asymmetric internal defects disrupt stacking and backbone regularity more than symmetric loops, which increases the relative accessibility of adjoining regions.

The reactivity of decoupled helices and helical termini extends further in the 5′ direction relative to a loop (equivalent to the 3′ helix end), although the position 3′ of the defect (equivalent to the 5′ helix end) is the most accessible individual purine (Fig. 5A). These two phenomena are consistent with simple considerations of A-form geometry. Although the minimum distance between phosphates across the major groove is approximately 10 Å for 7 bp (yielding a 4 Å groove width), this distance increases to 18 Å (12 Å groove width) for phosphates across a single base pair (8). Base pairs in an RNA helix are tilted approximately 19° relative to the helix axis. Thus, bases near the 3′ helix terminus protrude from the occluding major groove envelope, which increases their accessibility (Fig. 5A). The occurrence of the strongest modification at the 5′ base may reflect differences in stacking interactions, as shown in Fig. 5B. Whereas the 3′ base stacks on the base pair below it, the terminal 5′ base projects forward from the floor of the major groove, which increases its relative accessibility.

Given that the major groove is accessible at regions of unequal helicity and least accessible in continuous duplexes, we propose a low activation energy recognition switch, illustrated in Fig. 6. Coaxially stacked duplexes (like those found in the tRNA acceptor stem) may retain the regular helicity associated with resistance to attack by DEPC (Fig. 3); stacking could then be modulated by conformational changes within the RNA or by protein binding to reveal a major groove interaction site. Such an accessibility switch provides a nearly isoenergetic mechanism to regulate binding energies for major groove recognition and might contribute to cooperativity in such systems.

Long, regular uninterrupted helices in ribosomal, small nuclear, catalytic, and protein binding site RNAs are rare. A typical element of local RNA structure, an 8-bp segment incorporating a bulge or mismatch, for example, might feature a major groove accessible at almost every base pair. Major groove accessibility may be modulated more by coaxial stacking and other details of the RNA fold than by the intrinsic accessibility of isolated helices.

REFERENCES AND NOTES

1. C. J. Alden and S.-H. Kim, *J. Mol. Biol.* **132**, 411 (1979).
2. N. C. Seeman, J. M. Rosenberg, A. Rich, *Proc. Natl. Acad. Sci. U.S.A.* **73**, 804 (1976).
3. S.-H. Kim, *Prog. Nucleic Acid Res. Mol. Biol.* **17**, 181 (1976).
4. F. Michel, M. Hanna, R. Green, D. P. Bartel, J. W. Szostak, *Nature* **342**, 391 (1989); M. D. Been and A. T. Perrotta, *Science* **252**, 434 (1991); M. Yarus, M. Illangesekar, E. Christian, *Nucleic Acids Res.* **19**, 1297 (1991).
5. M. Ruff *et al.*, *Science* **252**, 1682 (1991).
6. K. M. Weeks and D. M. Crothers, *Cell* **66**, 577 (1991); correction, *ibid.* **70**, 1069 (1992).
7. J. D. Puglisi, R. Tan, B. J. Calnan, A. D. Frankel, J. R. Williamson, *Science* **257**, 76 (1992).
8. C. A. G. Haasnoot *et al.*, *J. Biomol. Struct. Dyn.* **3**, 843 (1986).
9. D. A. Peattie, *Proc. Natl. Acad. Sci. U.S.A.* **76**, 1760 (1979); ——— and W. Gilbert, *ibid.* **77**, 4679 (1980); A. Vincze, R. E. L. Henderson, J. J. McDonald, N. J. Leonard, *J. Am. Chem. Soc.* **95**, 2677 (1973).
10. S. R. Holbrook and S.-H. Kim, *Biopolymers* **22**, 1145 (1983).
11. A. E. Peritz, R. Kierzek, N. Sugimoto, D. H. Turner, *Biochemistry* **30**, 6428 (1991).
12. Oligoribonucleotides were synthesized chemically by standard protocols and purified to single nucleotide resolution by denaturing electrophoresis on 20% gels. The concentration of RNA eluted from the gel was determined with calculated extinction coefficients [G. D. Fasman, Ed., *Handbook of Biochemistry and Molecular Biology* (CRC Press, Cleveland, OH, ed. 3, 1975), p. 589]. All melting and chemical modification experiments were performed in 10 mM phosphate (pH 7.5), 200 mM NaCl, and 0.2 mM EDTA.
13. K. M. Weeks and D. M. Crothers, unpublished results.
14. Melting curves were obtained with a computer-interfaced Cary 1 spectrophotometer (Varian Instruments, Sugar Land, TX) with degassed 1.3-ml samples at a heating rate of 1°C per minute. Absorbance was monitored at 258 nm in a cell with a 1-cm path length for 1 μM samples in duplex (2 μM total strand concentration). Data were collected every 0.5°C, smoothed over 2.5°C, and after upper and lower base lines were subtracted, converted to fraction duplex (θ) as a function of temperature (T). We determined van't Hoff transition enthalpies (ΔH°_{vH}) and melting temperatures (T_m) by explicitly fitting the data to equation 3 given by J. Gralla and D. M. Crothers [*J. Mol. Biol.* **78**, 301 (1973)] solved for $\partial\theta/\partial T$ as a function of ΔH°_{vH} and T_m by substitution of the equilibrium expression and integrated form of the van't Hoff equation. Melting temperatures and enthalpies were reproducible to ±0.5°C and ±7%, respectively. Complete thermodynamic parameters for helix formation, typical differential melting transitions, and a description of the fitting procedure are available from the authors on request.
15. C. E. Longfellow, R. Kierzek, D. H. Turner, *Biochemistry* **29**, 278 (1990); J. SantaLucia, R. Kierzek, D. H. Turner, *ibid.* **30**, 8242 (1991).
16. H. Jacobson and W. H. Stockmayer, *J. Chem. Phys.* **18**, 1600 (1950); C. R. Cantor and P. R. Schimmel, *Biophysical Chemistry* (Freeman, New York, 1980), pp. 1205–1208. The entropy of loop closure, ΔS_{loop}, is defined as

$$\Delta S_{loop} = -cR\ln n + \Delta S_{geo}$$

Its relation to $\Delta\Delta G^\circ$ is defined as

$$\Delta\Delta G^\circ = -T\Delta S_{loop}$$

The length dependence (n) on loop formation is a function of the first term only; ΔS_{geo} is constant and reflects the geometric requirement for closure that the loop ends be close in space; R is the gas constant. The JS exponent, c, is 1.5 for a Gaussian chain, for which the theory is exact. For stiff, self-avoiding chains like RNA, c is usually set equal to 1.75.
17. Reactions at 20°C contained the purine strand at a final concentration of 1 μM, a low concentration of 5′ ^{32}P-labeled RNA, and the pyrimidine strand at the concentration (1.5 μM) required to form the duplexes shown (Figs. 1 and 4). Reactions were initiated by the addition of DEPC to 10% (in soluble excess) and vigorous vortexing (4 s); water replaced DEPC in control reactions. Duplex reactions were vortexed every 10 min; reactions of single-stranded and duplex RNAs were quenched after 10 and 60 min, respectively, by precipitation with three volumes of 5% (v/v) 3 M sodium acetate (pH 6) in ethanol at −70°C. The reactions were subsequently processed as described (*6*) and resolved by denaturing electrophoresis in 25% (w/v acrylamide, 20:1 acryl: bis, 6 M urea, 90 mM tris-borate, and 2 mM EDTA) gels.
18. We calculated probabilities of cleavage (l_i) by dividing the intensity at a given position (quantified with a Molecular Dynamics Phosphoimager) by the summed intensity of the band and all bands that corresponded to longer chains, including uncleaved material [L. C. Lutter, *J. Mol. Biol.* **124**, 391 (1978)]. After subtracting the probability of background cleavage, we determined accessibilities at single time points of reaction with DEPC:

$$\alpha_i = (l_i^{ds}/l_i^{ss})\cdot(1/6)$$

The factor 1/6 simply accounts for the different times that the reactions with single-stranded and double-stranded RNAs were incubated with reagent (*17*).
19. C. S. Chow, K. M. Hartman, S. L. Rawlings, P. W. Huber, J. K. Barton, *Biochemistry* **31**, 3534 (1992).
20. Values for K_{fray} were estimated from thermodynamic parameters derived from a nearest neighbor model determined with 1 M NaCl [S. M. Freier *et al.*, *Proc. Natl. Acad. Sci. U.S.A.* **83**, 9373 (1986)]. Values for K_{fray} were calculated with 200 mM NaCl by assuming ΔH° is independent of salt concentration and $\partial T_m/\partial\log[\mathrm{NaCl}] = 11$ (*13*).
21. M. A. Rould, J. J. Perona, D. Söll, T. A. Steitz, *Science* **246**, 1135 (1989); M. A. Rould, J. J. Perona, T. A. Steitz, *Nature* **352**, 213 (1991).

22. We thank S. Strobel and J. Doudna for helpful comments on the manuscript. Supported in part by NIH grant GM21966.

1 April 1993; accepted 12 July 1993